



# Parallel Synthesis of Poly(amino ether)-Templated Plasmonic Nanoparticles for Transgene Delivery

James Ramos,<sup>†</sup> Thrimoorthy Potta,<sup>‡</sup> Olivia Scheideler,<sup>§</sup> and Kaushal Rege<sup>\*,‡</sup>

<sup>†</sup>Biomedical Engineering, School of Biological and Health Systems Engineering, Arizona State University, Tempe, Arizona 85287-6106, United States

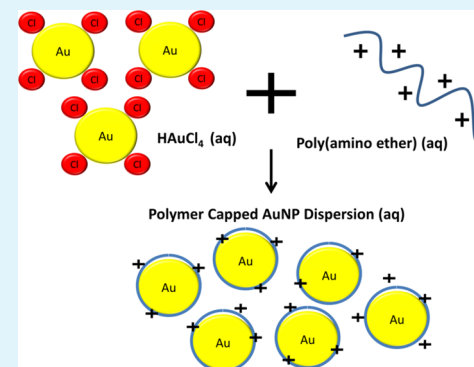
<sup>‡</sup>Chemical Engineering, School for Engineering of Matter, Transport, and Energy, Arizona State University, Tempe, Arizona 85287-6106, United States

<sup>§</sup>Department of Biological Systems Engineering, University of Nebraska—Lincoln, Lincoln, Nebraska 68583-0726, United States

## Supporting Information

**ABSTRACT:** Plasmonic nanoparticles have been increasingly investigated for numerous applications in medicine, sensing, and catalysis. In particular, gold nanoparticles have been investigated for separations, sensing, drug/nucleic acid delivery, and bioimaging. In addition, silver nanoparticles demonstrate antibacterial activity, resulting in potential application in treatments against microbial infections, burns, diabetic skin ulcers, and medical devices. Here, we describe the facile, parallel synthesis of both gold and silver nanoparticles using a small set of poly(amino ethers), or PAEs, derived from linear polyamines, under ambient conditions and in absence of additional reagents. The kinetics of nanoparticle formation were dependent on PAE concentration and chemical composition. In addition, yields were significantly greater in case of PAEs when compared to 25 kDa poly(ethylene imine), which was used as a standard cationic polymer. Ultraviolet radiation enhanced the kinetics and the yield of both gold and silver nanoparticles, likely by means of a coreduction effect. PAE-templated gold nanoparticles demonstrated the ability to deliver plasmid DNA, resulting in transgene expression, in 22Rv1 human prostate cancer and MB49 murine bladder cancer cell lines. Taken together, our results indicate that chemically diverse poly(amino ethers) can be employed for rapidly templating the formation of metal nanoparticles under ambient conditions. The simplicity of synthesis and chemical diversity make PAE-templated nanoparticles useful tools for several applications in biotechnology, including nucleic acid delivery.

**KEYWORDS:** gold nanoparticles, silver nanoparticles, nonviral gene delivery, photoreduction, combinatorial synthesis, transfection, inorganic nanoparticles



## INTRODUCTION

Plasmonic metal-based nanomaterials have been widely investigated as therapeutic and imaging agents<sup>1–3</sup> in biomedical studies and have also found applications in sensing and catalysis. In particular, gold nanoparticles (GNPs) have been increasingly investigated for separations,<sup>4</sup> sensing,<sup>5,6</sup> delivery of chemotherapeutic drugs<sup>7</sup> and nucleic acids,<sup>8–12</sup> and bioimaging.<sup>13–15</sup> Gold nanoparticles exhibit high surface-area-to-volume ratios and biocompatibility, are candidates for facile surface modification and functionalization, and possess unique optical properties.<sup>16</sup> Silver nanoparticles (AgNPs) demonstrate antibacterial activity resulting in potential application in treatments against microbial infections, burns, diabetic skin ulcers, and medical devices; the antimicrobial spectrum of AgNPs is considered to be broader than that of most common antibiotics.<sup>17</sup> AgNPs have also been investigated as antifungal agents<sup>18</sup> and as effective virucidal agents.<sup>19</sup> However, broad use of silver nanoparticles is somewhat limited due to concerns regarding their toxicity.<sup>20,21</sup>

Both GNPs and AgNPs have been synthesized using diverse methods, including chemical<sup>22–24</sup> or photochemical<sup>25–27</sup> reduction, and one-pot synthesis methods in which a polypeptide<sup>28</sup> or polymer acts as both a reducing and a capping agent.<sup>29–31</sup> Combinatorial and parallel synthesis methods allow exploration of diverse chemical space, leading to the rapid generation of molecular species for diverse applications. Although combinatorial methods have been widely employed for synthesis of small and macromolecules, their utility for nanoparticle synthesis is underexplored.

Amine-containing compounds, including amino acids and polymers, have been utilized as both reducing and stabilizing agents for the synthesis of GNPs.<sup>29,32–34</sup> We have recently reported the synthesis and use of polyamine-based poly(amino-ether) (PAE) cationic polymers<sup>35–37</sup> for transgene expression

Received: March 20, 2014

Accepted: August 1, 2014

Published: August 1, 2014

following delivery of plasmid DNA, and for enhancing adenoviral delivery to cells resistant to viral transduction.<sup>38,39</sup> In this study, we investigate the efficacy of a small set of cationic PAEs to template the formation of gold and silver nanoparticles in a one-pot, parallel synthesis reaction scheme under ambient conditions and compare nanoparticle formation efficacy to that observed with 25 kDa poly(ethylene imine) or pEI25k, a cationic polymer typically employed for delivering genes to mammalian cells. Identification of polymers that can template nanoparticle synthesis under ambient conditions, without the necessity of additional reducing agents, derivatization chemistries, or harsh synthesis conditions, offers significant advantages over other existing methods, particularly over those that utilize pEI25k. Poly(amino ether)-templated gold nanoparticle assemblies were also employed for transgene (plasmid DNA) delivery and expression in mammalian cells. Our current approach resulted in the identification of poly(amino ethers) that can simultaneously template nanoparticle formation and stabilize nanoparticles in aqueous media, resulting in the formation of PAE–GNP nanoassemblies, which, in turn, can deliver nucleic acids to mammalian cells.

## EXPERIMENTAL SECTION

**Poly(amino ether) (PAE) Synthesis.** A small set of eight PAE polymers, synthesized as described previously,<sup>35,37</sup> was used to demonstrate the combinatorial nanoparticle templating/synthesis approach. Briefly, 1,4-cyclohexanedimethanol diglycidyl ether (1,4C) was reacted in equimolar amounts with 1,4-bis(3-aminopropyl) piperazine (1,4Bis), 3,3'-diamino-N-methyldipropylamine (3,3'), pentaethylenehexamine (PHA), 1,3-diaminopropane (1,3DPP), and 2-methylpentane-1,5-diamine (2M1,5P), resulting in the formation of 1,4C–1,4Bis, 1,4C–3,3', 1,4C–PHA, 1,4C–1,3DPP, and 1,4C–2M1,5P PAEs, respectively. Neopentylglycol diglycidyl ether (NPGDE) was reacted in equimolar amounts with 1,4Bis, 3,3', PHA, and 1,3DPP to generate NPGDE–1,4Bis, NPGDE–3,3', NPGDE–PHA, and NPGDE–1,3DPP, respectively. Amine monomers employed in this study are shown in Figure 1a. The polymerization reaction was carried out in 20 mL glass scintillation vials for 16 h. Following the reaction, polymers were dissolved at a concentration of 10 mg/mL in phosphate-buffered saline (0.01× PBS), and the solution pH was adjusted to 7.4 using 30% hydrochloric acid in deionized (DI) water to compensate for the basicity of the cationic PAEs. The extent of polymerization was determined by comparing reactive amine concentrations at initial mixing of monomer reagents (time, 0 h) and after 16 h polymerization using the ninhydrin assay as described previously.<sup>35,38</sup>

**Synthesis of Poly(amino ether)–Gold Nanoparticles (PAE–GNPs) and Poly(amino ether)–Silver Nanoparticles (PAE–AgNPs) Synthesis.** PAE–GNP and PAE–AgNP syntheses were carried out in a one-pot reaction under ambient conditions. Briefly, 1 mg of HAuCl<sub>4</sub> or 0.1 mg of AgNO<sub>3</sub> was coincubated with each of the PAE polymers or branched pEI25k [25 kDa poly(ethyleneimine)] at polymer/metal salt weight ratios of 25:1, 50:1, and 100:1. Reactions were allowed to proceed in the dark at room temperature for 5 and 4 days for GNP and AgNP syntheses, respectively. Nanoparticle synthesis was monitored by measuring the solution absorption spectra from 300 to 999 nm in 5 nm increments at various times during the nanoparticle synthesis. After the monitoring period, PAE–nanoparticle dispersions were centrifuged for 20 min at 10 000 rcf to remove excess polymer and metal salt, redispersed in nanopure water, and filtered with a 0.22 μM filter for further characterization.

**Ultraviolet Irradiation.** To determine the effect of ultraviolet (UV) irradiation on nanoparticle formation, we coincubated 1 mg of metal salt or 0.1 mg AgNO<sub>3</sub> with each of the PAEs or branched pEI25k at polymer/metal salt weight ratios of 25:1, 50:1, and 100:1. Dispersions were then irradiated with a UV light using a hand-held UV lamp (366 nm, 6 W) for 24 and 3 h at room temperature for GNP and AgNP

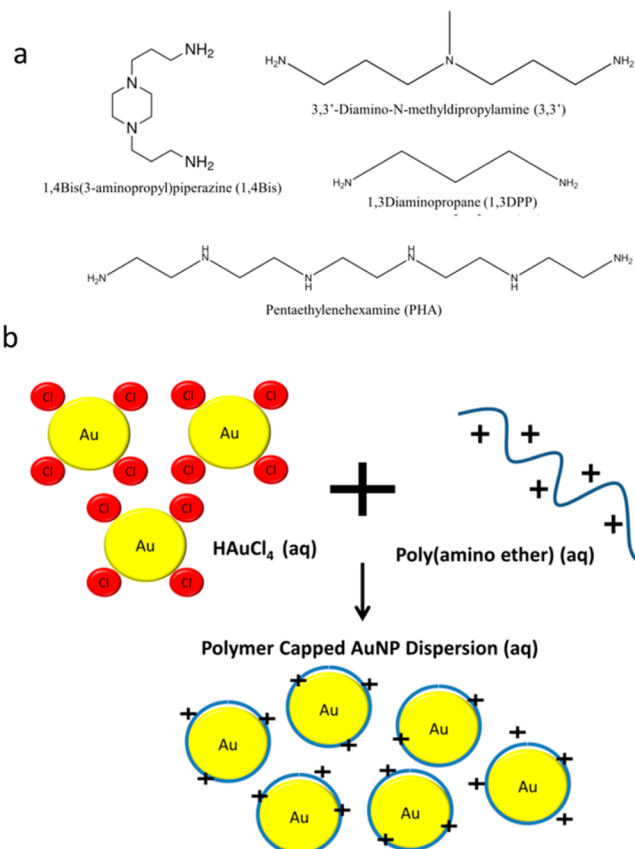


**Figure 1.** (a) Chemical structure of amine-containing monomers used in the synthesis of PAEs for nanoparticle formation. Abbreviations used in this study are in parentheses. (b) Simplified schematic of GNP synthesis using poly(amino ethers).

synthesis, respectively. Following irradiation, dispersions were allowed to sit for an additional 4 days or 21 h in the dark at room temperature for GNP or AgNP syntheses, respectively. To monitor nanoparticle formation, we monitored the solution absorption spectra from 300 to 999 nm in 5 nm increments at various times. After 5 days or 24 h for GNP or AgNP syntheses, respectively, dispersions were centrifuged for 20 min at 10 000 rcf to remove excess polymer and metal salt, redispersed in nanopure water, and filtered through a 0.22 μM filter for further characterization.

**Transmission Electron Microscopy.** Following synthesis, PAE–GNP and PAE–AgNPs were visualized using transmission electron microscopy (TEM), which was carried out using a JEOL-JEM-2000FX microscope, operating at 200 kV (Leroy Eyring Center for Solid State Sciences, Arizona State University). Specimen samples for TEM were prepared by casting a drop of PAE–GNP or PAE–AgNP dispersions onto a carbon film on a 200 mesh copper wire screen (Global Electron Microscopy Technology Co.) and dried in air. Dried samples were examined by TEM at 200 kV.

**Determination of Hydrodynamic Diameter and Zeta Potential of PAE–GNPs and PAE–AgNPs.** The hydrodynamic diameters of PAE–GNPs and PAE–AgNPs were determined via dynamic light scattering (DLS) using a particle sizer (Corvus Advanced Optical Instruments). Hydrodynamic diameters are reported in nanometers (nm). 1,4C–1,4Bis–GNPs were synthesized at a ratio of 100:1 of 1,4C–1,4Bis/HAuCl<sub>4</sub> under UV irradiation. Tempered GNPs were set to concentrations of 4.9, 9.8, 24.4, 48.8, or 97.5 μg/mL and loaded with between 0 and 250 ng of pGL3 plasmid DNA. Dispersions were transferred into folded capillary zeta cells (Malvern, Westborough, MA). Zeta potential values were determined using a Zetasizer Nano ZS (Malvern).

**Determination of Primary and Secondary Amine Concentration of PAE–GNPs.** Ninhydrin (2,2-dihydroxyindane-1,3-dione)

reacts with free primary and secondary amines with a resulting deep blue or purple color, which can be measured and compared to a standard for quantifying reactive (i.e., primary and secondary) amine concentrations. Glycine standards, with known amine concentrations (0, 50, 150, and 300  $\mu\text{M}$ ), were prepared in nanopure water with a total volume of 200  $\mu\text{L}$ . GNPs were synthesized as described above. Following synthesis, GNPs were dispersed in nanopure water, and their optical density was determined at the maximum absorbance wavelength. GNP dispersions of 200, 100, and 75  $\mu\text{L}$  were prepared and filled up to 200  $\mu\text{L}$  with nanopure water. Following the addition of the ninhydrin reagent (100  $\mu\text{L}$ ), all samples were incubated in water at 100 °C for 10 min, following which, they were allowed to cool to room temperature. We then added 500  $\mu\text{L}$  of 95% ethanol to each sample and measured the absorbance at 570 nm. Reactive amine concentrations were determined by comparing measured values to the glycine standard curve. Amine concentrations were then normalized to the respective GNP maximum absorbance (pseudo-concentration).

**Plasmid DNA Delivery Using 1,4C–1,4Bis–GNPs.** *Plasmid DNA.* The pGL3 control vector (Promega Corp., Madison, WI), which encodes for the modified firefly luciferase protein under the control of an SV40 promoter, was used for transgene expression studies. *Escherichia coli* (XL1 Blue) cells containing the pGL3 plasmid DNA were cultured overnight (16 h, 37 °C, 150 rpm) in 15 mL tubes (Fisher) containing 5 mL of Terrific Broth (MP Biomedicals, LLC). The cultures were then centrifuged at 5400g and 4 °C for 10 min. Plasmid DNA was purified according to the QIAprep Miniprep Kit (Qiagen) protocol. DNA concentration and purity were determined on the basis of absorbance at 260 and 280 nm using a NanoDrop spectrophotometer (ND-1000; NanoDrop Technologies). Plasmid DNA concentrations of 200–300 ng/ $\mu\text{L}$  were typically obtained, and volumes were adjusted in order to load between 10 and 200 ng of pGL3 plasmid DNA on 1,4C–1,4Bis–GNPs prior to transfections.

*Cell Culture.* 22Rv1 human prostate cancer cells and MB49 murine bladder cancer cells were both generous gifts from Professor Christina Voelkel-Johnson of the Medical University of South Carolina as part of an existing collaboration. RPMI-1640 with L-glutamine and HEPES (RPMI-1640 medium), DMEM with high glucose, L-Glutamine, and HEPES, Pen-Strep solution: 10 000 units/mL penicillin and 10 000  $\mu\text{g}/\text{mL}$  streptomycin in 0.85% NaCl, and fetal bovine serum (FBS), were purchased from Hyclone. Serum-free medium (SFM) consisted of RPMI-1640 or DMEM medium plus 1% Pen-Strep (1000 units/mL penicillin and 1000  $\mu\text{g}/\text{mL}$ ). Serum-containing medium (SCM) consisted of SFM plus 10% FBS. 22Rv1 cells, as received, were cultured in a 5% CO<sub>2</sub> incubator at 37 °C using RPMI-1640 medium containing 10% heat-inactivated FBS and 1% antibiotics (Pen-Strep). MB49 cells, as received, were cultured in a 5% CO<sub>2</sub> incubator at 37 °C using DMEM containing 10% heat-inactivated FBS and 1% antibiotics (Pen-Strep).

*Cytotoxicity.* Cytotoxicity of 1,4C–1,4Bis–GNPs was determined in 22Rv1 and MB49 cells. Cells were seeded at a density of 8400 cells/well in 150  $\mu\text{L}$  of SCM in a 96-well plate and allowed to attach overnight. Plasmid DNA (pGL3) encoding the luciferase protein was diluted to a concentration of 50 ng/ $\mu\text{L}$  using Tris EDTA buffer (10 mM Trizma and 1 mM EDTA, Thermo Fisher Scientific, Rockford, IL). 1,4C–1,4Bis–GNPs were dispersed in SFM at concentrations of 4.9, 9.8, 24.4, 48.8, and 97.5  $\mu\text{g}/\text{mL}$ . 1,4C–1,4Bis–GNP dispersions were then coincubated with 0, 25, 50, 75, 100, 125, 150, 200, or 250 ng of pGL3 plasmid DNA for 30 min. Following the incubation period, pGL3 plasmid-loaded 1,4C–1,4Bis–GNPs were used to treat 22Rv1 or MB49 cells in SFM for 6 h in an incubator under humidified air containing 5% CO<sub>2</sub> at 37 °C. Subsequently, the medium was replaced with fresh SCM. Lipofectamine-3000 (Lipo3000) complexes were prepared according to manufacturer's protocol using the same plasmid DNA amounts used for 1,4C–1,4Bis–GNP experiments and used to treat cells. After cells were incubated for 48 h, cell viability was determined using the 3-(4,5-dimethylthiazol-2-yl)-2,5-diphenyltetrazolium bromide (MTT) cell proliferation assay kit (ATCC). This assay involves the enzymatic conversion of the MTT substrate to purple-colored formazan in metabolically active cells. This activity is widely

employed as an indicator of cell viability and proliferation;<sup>40</sup> loss of metabolic activity was used as an indirect indicator of loss of cell viability. Following the addition of the MTT reagent (2 h at 37 °C), cells were treated with a lysis buffer from the kit and kept at room temperature in the dark for 2 h in order to lyse cells and solubilize the MTT product. The absorbance of each well was measured using a plate reader (BioTek Synergy 2) at 570 nm to assay for the blue-colored MTT product. Absorbance readouts were normalized to the live (untreated) and dead (5  $\mu\text{L}$  of 30% hydrogen peroxide-treated) controls in subsequent data analyses.

*Transgene Delivery and Expression.* MB49 and 22Rv1 cells were transfected using pGL3 plasmid-loaded 1,4C–1,4Bis–GNPs, as described above. Prior to transfection, cells were seeded at a density of 8400 cells/well in 150  $\mu\text{L}$  of SCM in a 96-well plate and allowed to attach overnight. The pGL3 plasmid encoding the luciferase protein was diluted to a concentration of 50 ng/ $\mu\text{L}$  using Tris EDTA buffer (10 mM Trizma and 1 mM EDTA, Thermo Fisher Scientific, Rockford, IL). 1,4C–1,4Bis–GNPs were dispersed in SFM at concentrations of 4.9, 9.8, 24.4, 48.8, and 97.5  $\mu\text{g}/\text{mL}$ . 1,4C–1,4Bis–GNP dispersions were then coincubated with 0, 25, 50, 75, 100, 125, 150, 200, or 250 ng of pGL3 plasmid DNA for 30 min. Following incubation, pGL3 loaded 1,4C–1,4Bis–GNPs were used to treat 22Rv1 or MB49 cells in SFM for 6 h in an incubator under humidified air containing 5% CO<sub>2</sub> at 37 °C. Subsequently, the medium was replaced with fresh SCM and allowed to incubate for an additional 48 h. Lipo3000 complexes were prepared according to manufacturer's protocol using the same plasmid DNA amounts used for 1,4C–1,4Bis–GNP experiments and used to treat cells. Luciferase protein expression, expressed in terms of relative luminescence units, or RLU, was determined using the luciferase assay kit according to the manufacturer's protocol 48 h after transfection; luminescence measurements were carried out using a plate reader (Bio-Tek Synergy 2). The protein content (mg protein) in each well was determined using the BCA Protein Assay Kit. Transgene (luciferase) expression in all cell lines was calculated, normalized with the protein content, and expressed as RLU per milligram (mg) protein (RLU/mg protein). Transfection experiments were performed at least in triplicate.

*Statistical Analyses.* For cytotoxicity and transgene expression studies, PAE-templated GNP were compared to Lipo3000 at the same plasmid DNA loading conditions (Student's *t* test, \* *p* ≤ 0.05, \*\* *p* ≤ 0.01). Data represent mean ± standard error.

## RESULTS

A focused library of poly(amine ethers) (PAEs; reaction scheme shown in Figure S1, Supporting Information) was previously synthesized, characterized, and investigated for transgene delivery capabilities.<sup>35,37</sup> Several candidates among the new PAEs synthesized in our laboratory demonstrated higher transgene expression efficacies compared to 25 kDa poly(ethylene imine), or pEI25k. In addition, the facile synthesis method and chemical diversity of these amine-containing polymers further facilitates the combinatorial synthesis of plasmonic nanoparticles (GNP and AgNPs) under ambient conditions, without the need for energy intensive conditions or other reducing agents. PAEs were able to template and cap nanoparticles, leading to stable PAE–nanoparticle dispersions in aqueous media. The diversity in PAE chemistry translates to differences in the yield and kinetics of formation of these nanoparticles. PAE-templated gold nanoparticles were employed for transgene delivery and expression in mammalian cells.

**Kinetics of Nanoparticle Formation. Gold Nanoparticle (GNP) Formation.** GNP formation was observed for all polymers and conditions following incubation of PAEs with HAuCl<sub>4</sub> for 5 days (Figures 2 and 3 and Figure S2, Supporting Information). Nanoparticle formation was visualized by a change in color from a pale yellow solution to red/maroon-

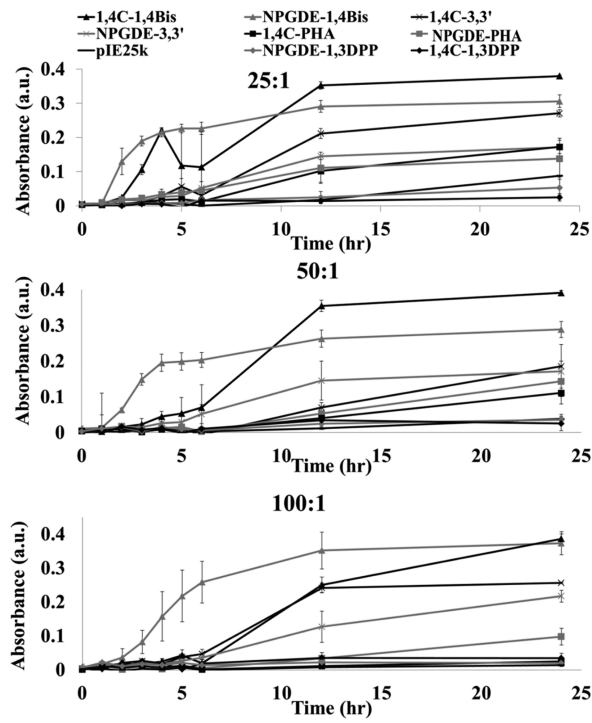


**Figure 2.** Kinetics of PAE-templated GNP synthesis in the absence of UV irradiation monitored at maximum absorption wavelength (500–540 nm) at polymer/HAuCl<sub>4</sub> weight ratios of (top) 25:1, (middle) 50:1, and (bottom) 100:1. Nanoparticles were monitored for 5 days; however, only the first 24 h are shown. All particles were synthesized in triplicate, and data points represent the mean absorbance  $\pm$  standard error. Lines connecting data points are included for visualization only.

colored dispersion. This color change was corroborated by a light absorption peak maximum at approximately 520 nm, which is characteristic of spherical GNPs (Figure S3, Supporting Information).<sup>31</sup> The mechanism of gold nanoparticle formation is hypothesized to occur by metal ion binding to the amines present in PAEs. Following binding, transfer of electrons from the amines to metal ions<sup>29</sup> causes reduction of the latter to zerovalent ions. This leads to nucleation, growth, and subsequent nanoparticle formation. As a result, PAEs are integral to this process because they can template and cap nanoparticle formation, leading to the formation of stable dispersions in aqueous media (Figure 1b).

As seen in Figure 2, the extent of nanoparticle formation depends on the polymer chemistry employed. These observed differences in PAE-templated nanoparticle formation rates can, in turn, be correlated to the chemical composition of the amine monomers used for the polymer synthesis (Figure 1). Both 1,4Bis and 3,3'-based polymers exhibited the fastest rates of nanoparticle formation. Although there was an observed decrease in the absorbance of 1,4C-1,4Bis-templated GNP samples (25:1) after  $\sim$ 4 h, likely due to aggregation or precipitation, the final absorbance or nanoparticle concentration in the case of the 1,4C-1,4Bis polymer outperformed other polymers under the same conditions. The 1,4-bis(3-aminopropyl) piperazine (1,4Bis) monomer contains two primary amines (with one or both converted to a secondary amine following polymer synthesis), in addition to two tertiary amines. Similarly, the 3,3'-diamino-N-methyldipropylamine (3,3') monomer, contains two primary amines (with one or

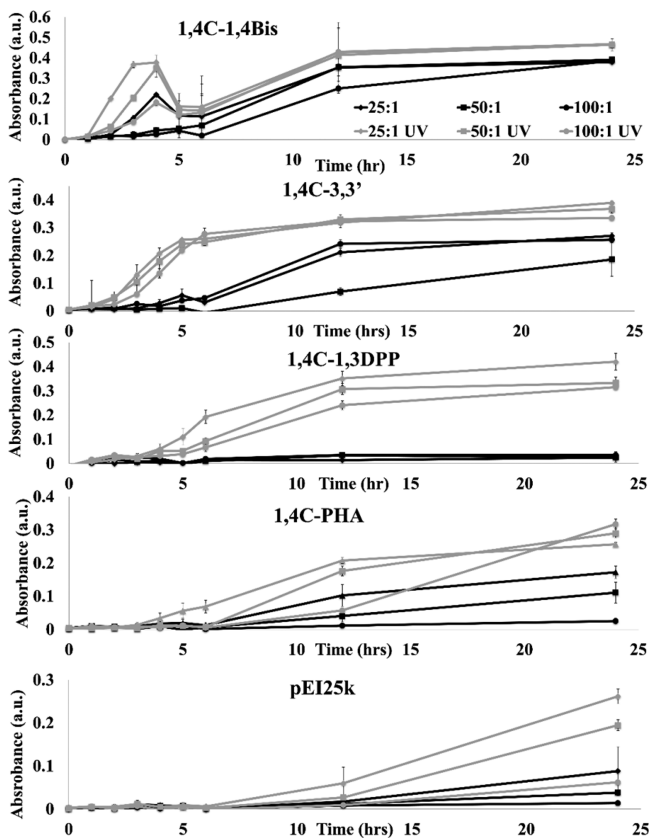


**Figure 3.** Comparison of 1,4C-derived PAE-templated GNP formation kinetics monitored at maximum absorption peak (500–540 nm) as a function of PAE/HAuCl<sub>4</sub> weight ratio. Nanoparticle synthesis in the absence of UV irradiation is replotted from Figure 2 to better visualize the difference of UV vs non-UV irradiation for each polymer. Nanoparticles were monitored for 5 days; however, only the first 24 h are shown. Data points represent the mean absorbance  $\pm$  standard error ( $n = 3$ ). Lines connecting individual data points are included for visualization only. Corresponding data for NPGDE-derived PAEs are shown in Figure S2 (Supporting Information).

both converted to a secondary amine following polymer synthesis) as well as a tertiary amine. It is accepted that the binding of tertiary amines to metals is weaker compared to primary or secondary amines.<sup>41</sup> The presence of tertiary amines in these polymers likely results in faster dynamics of binding, reduction, and release of gold ions. Faster nucleation and growth of gold nanoparticles is therefore likely observed in cases of polymers that have moderate affinities of interaction with gold<sup>42</sup> or those with an increased number of tertiary amines. PHA and pEI25k are both dominated by primary and secondary amines, whereas 1,3DPP has two primary amines. The high amine/charge density in pEI25k and PHA and the presence of primary amines in 1,3DPP may result in stronger binding to gold ions, resulting in decreased solvation and thus decreased nucleation, explaining the decreased kinetics of nanoparticle formation. In addition, complexation has been found to lower the redox potential of metal ions, resulting in decreased reducibility.<sup>42</sup> This suggests that polymers that are dominated by strong metal binding moieties (i.e., primary and secondary amines) will likely demonstrate strong binding and increased complexation times, resulting in reduced reduction of metal ions, and therefore decreased kinetics of nanoparticle synthesis. Our results therefore indicate that amine-containing polymers or molecules with high amounts of tertiary amines are

likely to demonstrate enhanced kinetics for generation of plasmonic nanoparticles. These observations also allow for the synthesis of polymers with controllable reducing properties for tunable nanoparticle growth kinetics. However, sophisticated molecular modeling methods (e.g., molecular dynamics simulations), subsequent syntheses, and structure–property analyses will be necessary to delve deeper into the mechanisms of PAE-templated nanoparticle formation.

An increase in the polymer/metal salt ratio resulted in retardation in the kinetics of nanoparticle formation, indicating that additional reduction/templating and capping sites did not promote faster kinetics (Figure 3). This difference in nanoparticle formation was observed during the first 12 h of incubation, whereas the effective concentrations of the GNP dispersions were comparable for a given templating polymer after 24 h. It has been reported that entanglement of polymer chains can decrease the complexation rate of polymers with metal ions,<sup>30</sup> which, in turn, can result in decreased reduction rates of metal ions and therefore account for the subsequent reduction in nanoparticle formation kinetics. Thus, in addition to identifying appropriate chemistries, it is also important to identify appropriate reaction conditions for nanoparticle synthesis. For example, it has been observed that increasing the reaction temperature can result in faster nanoparticle formation,<sup>43</sup> and modifying the reaction pH<sup>44</sup> or reagent addition rate<sup>45</sup> can result in different formation mechanism.

UV irradiation has been employed for photochemical reduction of both gold and silver ions for nanoparticle formation.<sup>25,26,46,47</sup> Exposure to UV irradiation for 24 h indeed resulted in an increase in GNP formations in all PAEs employed, but it was particularly effective in 1,3DPP and pEI25k polymers (Figure 3). In the presence of UV irradiation, formation of GNPs likely occurs through a coreduction mechanism in which gold ions are simultaneously reduced by both photo and chemical means. It has been proposed that nanoparticle formation following UV exposure occurs in a multistep process.<sup>48</sup> The proposed mechanism begins with excitation of Au<sup>3+</sup> ions by the incident UV radiation, followed by subsequent reduction to an unstable Au<sup>2+</sup> form. This results in disproportionation of Au<sup>2+</sup> resulting in the formation of Au<sup>1+</sup> and Au<sup>3+</sup>. The Au<sup>1+</sup> ions then absorb an additional photon and are again photoreduced to Au<sup>0</sup> or zerovalent gold ions, which nucleate and grow to form gold nanoparticles. It is likely that UV radiation enhances the kinetics of PAE-templated nanoparticle formation via mechanisms similar to those previously proposed.<sup>25,26</sup>

We also investigated nanoparticle formation in the presence of an anionic polymer, poly(styrenesulfonate), or PSS. To the best of our knowledge, PSS has no known inherent metal reducing capabilities, although the polymer has been employed as a stabilizing reagent in the presence of a reducing agent for nanoparticle synthesis.<sup>49–51</sup> Gold nanoparticle formation was observed following UV-based photoreduction of HAuCl<sub>4</sub> in the presence of PSS after 24 h (Figure S4, Supporting Information); no change in color (i.e., no nanoparticle formation) was observed when the gold salt was incubated with PSS in the absence of UV light (Figure S4, Supporting Information). These results indicate that UV irradiation can induce nanoparticle formation (metal reduction) in the presence of a suitable capping agent and that the observed increase in PAE nanoparticle formation in the presence of UV irradiation is most likely due to additional metal reduction via UV-photoreduction. In contrast to PSS, PAEs can template the

formation of gold nanoparticles by themselves in the absence of UV radiation. However, GNP kinetics and yield are further enhanced by exposure to UV radiation via a coreduction effect. All else being same, exposure to UV radiation resulted in higher yields of GNPs than with PAEs alone in the absence of UV radiation, as demonstrated by higher final optical densities (surrogate for nanoparticle concentration).

**Silver Nanoparticle (AgNP) Formation.** AgNP formation was observed for all PAE polymers and conditions following incubation of PAEs with AgNO<sub>3</sub> for 3 days at polymer/AgNO<sub>3</sub> weight ratios of 25:1, 50:1, and 100:1. Interestingly, AgNP formation was not observed in the case of pEI25k (Figures 4

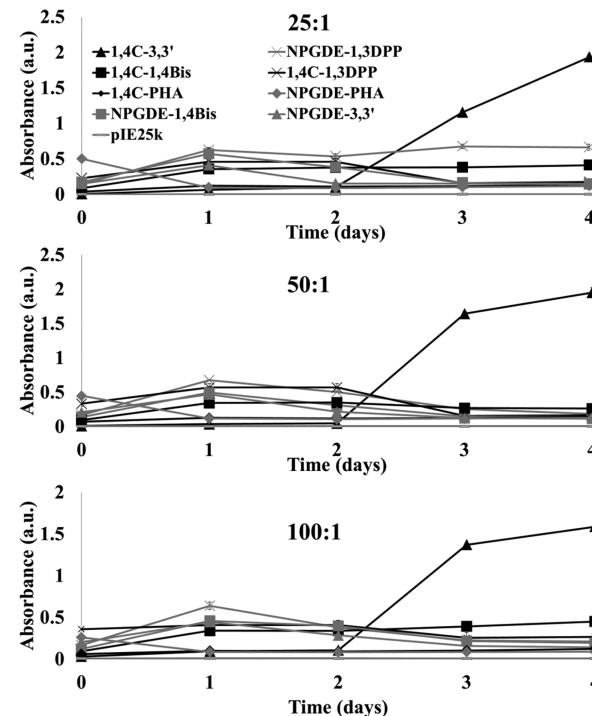


**Figure 4.** Kinetics of PAE-templated AgNP synthesis, in absence of UV radiation, monitored at maximum absorption peak (400–430 nm) at polymer/AgNO<sub>3</sub> weight ratios of (top) 25:1, (middle) 50:1, and (bottom) 100:1. Nanoparticles were monitored for 4 days. Data points represent the mean absorbance  $\pm$  standard error ( $n = 3$ ). Lines connecting data points are included for visualization only.

and S5, Supporting Information). Formation of AgNPs was visually observed by a change in solution color from clear to a yellow color, which was reflected in the appearance of a maximum absorption peak at approximately 420 nm (Figure S6, Supporting Information). However, the yields of AgNPs were lower than that of GNPs, and the times required for nanoparticle formation were significantly longer than those for GNPs. This may be a result of amines showing stronger affinities to silver than to gold,<sup>52</sup> resulting in stronger binding, decreased solvation, and lower levels of nanoparticle nucleation. Additionally, silver has lower reduction potential and higher electrochemical potential compared to gold, which may further explain the lower yield of AgNP formation.<sup>53</sup> With the exception of 1,4C-3,3' polymer, PAE-based systems showed a moderate increase in absorbance at approximately 420 nm (Figure 4). In fact, a reduction in maximal absorbance was observed from 24 to 48 h, likely due to aggregation and precipitation of the nanoparticles. Interestingly, color change or

appearance of an absorbance peak indicative of AgNP formation was not observed for pEI25k under any of the conditions investigated. This is likely due to strong binding of the metal ions to the primary and secondary amines of pEI25k, which does not allow for subsequent solvation and nanoparticle nucleation. Previous reports on pEI25k-templated AgNP formation employed a strong reducing agent (e.g., NaBH<sub>4</sub>)<sup>54</sup> or high incubation temperatures.<sup>55</sup> Here, we demonstrate that PAEs generated in our laboratory are capable of synthesizing and capping AgNPs in a one-pot synthesis method at room temperature without the use of an additional reducing agent. These results underscore the importance of combinatorial approaches to template identification; parallel screening of different PAEs rapidly resulted in the identification of chemistries that led to formation of stable plasmonic nanoparticle dispersions.

As with GNPs, PAE-mediated AgNP synthesis was investigated in the presence of UV-irradiation to determine if photoreduction could increase the kinetics and yield of nanoparticles. Whereas observable PAE-AgNP synthesis took 1–2 days without UV-irradiation, AgNP formation began within 1–5 min in the presence of UV irradiation (Figures 4 and 5 and Figure S5, Supporting Information). Interestingly,

AgNP formation was not observed in the case of pEI25K, even in the presence of UV irradiation, as indicated by a lack of color change and a lack of an absorption peak at 420 nm in the spectrum. To study the effects over a longer period of time and to allow for maximal AgNP formation, we exposed PAE-AgNO<sub>3</sub> solutions to UV radiation for a maximum of 3 h (Figures 5 and S5, Supporting Information), during which AgNP formation proceeded with fast kinetics. However, negligible levels of nanoparticle formation were observed once the UV irradiation was removed, and the nanoparticles were kept in the dark for an additional 21 h. These results indicate that the efficacy of photoreduction is significantly higher than that of chemo-reduction for AgNP formation. However, similar to observations with GNPs, AgNP formation occurred most rapidly at lower polymer/metal salt weight ratios. All PAEs demonstrated similar efficacies for templating and capping AgNPs, and aggregation/precipitation of AgNPs was not observed when UV-irradiation was employed, unlike in the absence of radiation. PHA-based polymers were an exception to this behavior, because nanoparticle precipitation was observed during AgNP synthesis, resulting in a decrease of the maximum absorbance over time.

**PAE-Nanoparticle Characterization. Transmission Electron Microscopy.** Following synthesis in the absence of UV-irradiation and removal of excess polymer and metal salts via centrifugation, 1,4C-1,4Bis-GNPs, NPGDE-1,4Bis-GNPs, pEI25k-GNPs, and NPGDE-1,4Bis-AgNPs were characterized by TEM; these PAEs were chosen because 1,4Bis-based PAEs demonstrate the fastest kinetics of GNP formation. 1,4C-1,4Bis-GNPs, NPGDE-1,4Bis-GNPs, and pEI25k-GNPs possessed spherical metal cores in the sub-20 nm range (Figure 6a–i). Despite the observed differences in the initial kinetics of nanoparticle formation, the metal cores exhibit similar sizes across the three different weight ratios tested. However, aggregation/bridging of some metal cores was observed in pEI25k-GNPs. The sizes of metal cores in NPGDE-1,4Bis-templated AgNPs are larger than 20 nm, with similar sizes across the three different tested weight ratios (Figure 6j–l). Some aggregation and, interestingly, formation of nanorods (cylindrical shapes) were observed in NPGDE-1,4Bis-AgNPs.

**Hydrodynamic Diameter.** The hydrodynamic diameters of all PAE-GNPs were in the sub-150 nm range (Figure 7a). The hydrodynamic diameter for a given PAE-GNP did not vary significantly with different PAE/gold salt weight ratios. However, the hydrodynamic diameter increased moderately with an increase in the weight ratio for 1,4C-1,4Bis and 1,3DPP PAE-templated gold nanoparticles. Interestingly, the hydrodynamic diameters decreased with increasing weight ratios for PHA-based polymers. With the exception of 1,4C-1,4Bis-GNPs, the hydrodynamic diameters of PAE-GNPs synthesized with and without UV-irradiation are comparable. pEI25k-GNPs exhibited the smallest hydrodynamic diameters in the 25–35 nm range, which was similar to the size observed via TEM. The hydrodynamic diameters of 1,4C-1,4Bis-GNPs and NPGDE-1,4Bis-GNPs (non-UV-irradiated) were much larger than the metal cores observed via TEM. This is likely due to the presence of the polymer/PAE coat, which was not observed in TEM analysis.

All PAE-AgNPs exhibited hydrodynamic diameters in the sub-120 nm range (Figure 7b); no measurements were obtained for pEI25K due to lack of nanoparticle formation. As opposed to GNPs, less clear trends in hydrodynamic

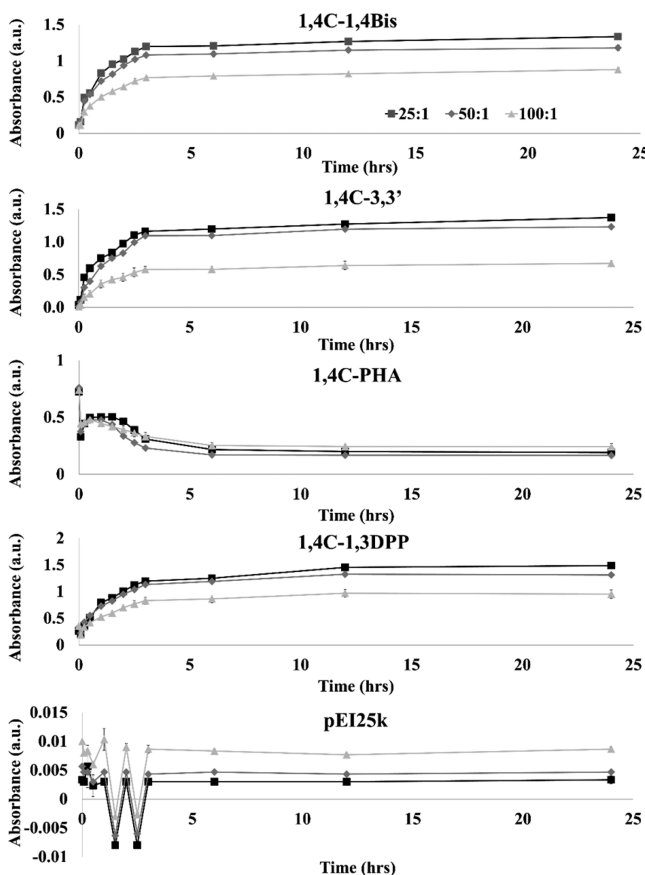


**Figure 5.** Kinetics of 1,4C-derived PAE-templated AgNP synthesis in the presence of UV-irradiation, monitored at maximum absorption peak (400–430 nm) at different polymer/AgNO<sub>3</sub> weight ratios. The PAE-AgNO<sub>3</sub> solution was subjected to UV radiation for the first 3 h, and nanoparticle formation was monitored for a total of 24 h. Data points represent the mean absorbance  $\pm$  standard error ( $n = 3$ ). Lines connecting individual data points are for visualization only. Corresponding data for NPGDE-derived PAEs are shown in Figure S5 (Supporting Information).

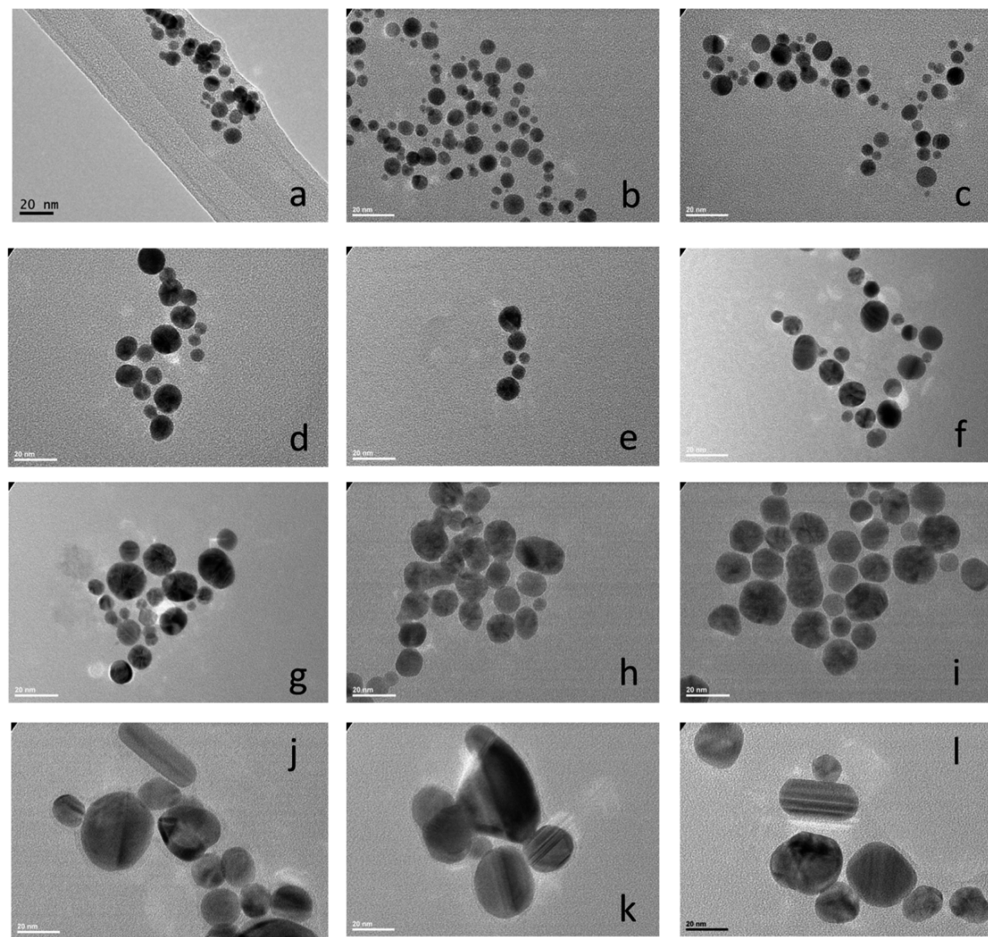


**Figure 6.** TEM images of 1,4C–1,4Bis-templated GNPs at a weight ratio of (a) 25:1, (b) 50:1, and (c) 100:1; NPGDE–1,4Bis–GNPs at weight ratios of (d) 25:1, (e) 50:1, and (f) 100:1; pEI25k–GNPs at weight ratios of (g) 25:1, (h) 50:1, and (i) 100:1; and NPGDE–1,4Bis–AgNPs at weight ratios of (j) 25:1, (k) 50:1, and (l) 100:1, polymer/HAuCl<sub>4</sub>. All scale bars indicate 20 nm.

diameter size were seen with respect to synthesis conditions (i.e., change in weight ratios or UV irradiation) in case of PAE-AgNPs. For example, in case of 1,4C–1,4Bis, 1,4C–1,3DPP, and NPGDE–PHA polymers, AgNPs synthesized in the presence of UV-irradiation are smaller in size than those synthesized in absence of the radiation. However, the opposite trend was observed in other PAEs such as, 1,4C–3,3' and NPGDE–1,3DPP polymers. Finally, diameters of AgNPs were comparable for some PAEs including 1,4C-PHA, NPGDE-1,4Bis, and NPGDE-3,3'.

**Amine Content.** PAE-GNPs were characterized for amine content using the ninhydrin assay to further confirm the presence of the cationic polymer in the nanoassemblies; higher amine content can be used as an indicator of increased polymer content. Similar to the trend in hydrodynamic diameters, at increased weight ratios of PAE to HAuCl<sub>4</sub>, 1,4C–1,4Bis–GNPs exhibited slightly increased amine content (i.e., increased polymer coating) (Figure 8). In addition, the amine content for PHA-based polymers decreased with an increase in weight ratios, which is in agreement with the decrease in hydrodynamic diameters observed for these polymers (Figure 7). Taken together, the amine content can be used as an indicator of extent of polymer coating, and follows similar trends as that of the measured hydrodynamic diameters.

**Biological Activity of PAE-Templated Nanoparticles: Transgene Delivery and Expression.** Previous studies from

our laboratory demonstrated that 1,4C–1,4Bis polyplexes,<sup>35,56</sup> and 1,4C–1,4Bis-coated gold nanorods,<sup>11</sup> were able to deliver plasmid DNA leading to transgene expression or gene silencing<sup>57</sup> in mammalian (e.g., cancer) cells. In these previous investigations, 1,4C–1,4Bis–plasmid DNA complexes (polyplexes) exhibited decreased cytotoxicity and up to 80-fold enhancement in transfection efficacies compared to pEI25k in PC3–PSMA cells at higher polymer/plasmid weight ratios. In a separate study, 1,4C–1,4Bis was employed to coat pre-made gold nanorods using a layer-by-layer deposition approach. These nanoparticles exhibited up to 165-fold enhancement compared to similarly modified pEI25k gold nanorods. Given the previously known activity of the 1,4C–1,4Bis–PAE, we investigated 1,4C–1,4Bis–GNP nanoassemblies for plasmid DNA delivery and subsequent transgene expression. It is important to mention that in previous cases, PAEs were employed to coat pre-made nanoparticles for plasmid DNA delivery, which is different from these current DNA delivery vehicles, which are essentially PAE-templated nanoparticles.

1,4C–1,4Bis–GNPs were synthesized at a weight ratio of 100:1 (1,4C–1,4Bis/HAuCl<sub>4</sub>) in the presence of UV irradiation, as described in the Experimental Section, and dispersed in SFM at different concentrations. 1,4C–1,4Bis–GNPs were then loaded with 1–250 ng of pGL3 plasmid DNA, which expresses the luciferase protein. Plasmid DNA-loaded 1,4C–1,4Bis–GNPs or “nanoassemblies” were delivered to

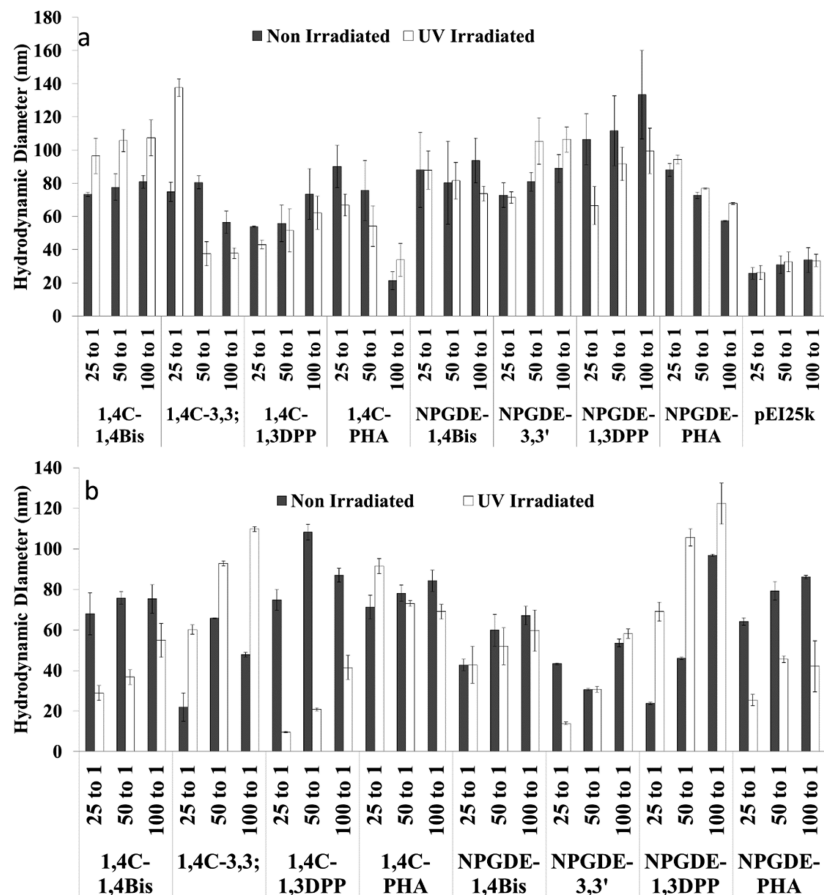


**Figure 7.** Hydrodynamic diameters of (a) PAE-GNPs and (b) PAE-AgNPs following synthesis at different weight ratios, with and without UV irradiation. Hydrodynamic diameters represent the mean hydrodynamic diameter  $\pm$  standard error ( $n = 3$ ).

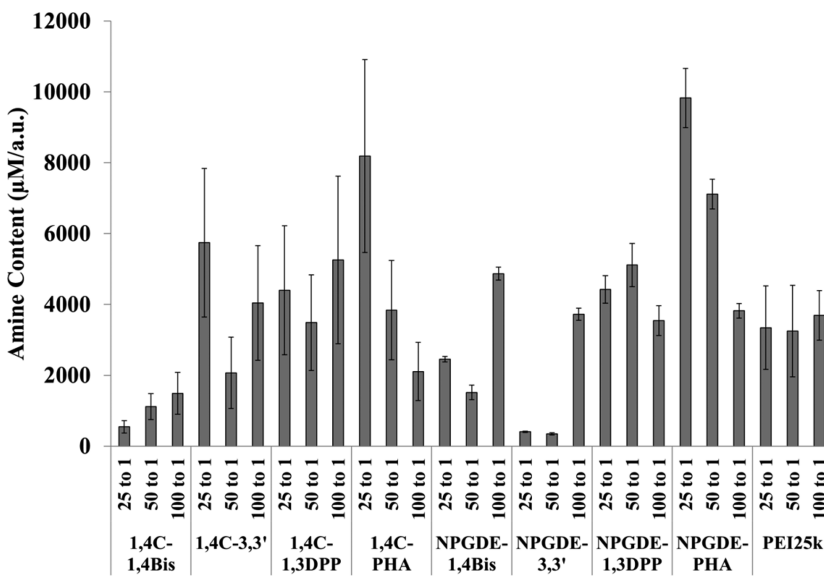


**Figure 8.** Amine concentrations of PAE-GNPs determined by the ninhydrin assay. Amine concentrations ( $\mu\text{M}$ ) are normalized by the maximum absorbance (a.u.) of the PAE-GNPs. Data points ( $n \geq 3$ ) represent the mean measurement  $\pm$  standard error.

22Rv1 human prostate cancer and MB49 murine bladder cancer cells in order to evaluate their transgene (luciferase) expression efficacies. Lipo3000 was also investigated as a commercially available delivery vehicle. The nanoassemblies exhibited greater cytotoxicity in 22Rv1 cells (Figure 9a) when compared to MB49 cells (Figure 9b). Lower concentrations of

1,4C-1,4Bis-GNPs were therefore used for delivery to 22Rv1 cells (concentrations of 4.9, 9.8, 24.4, and 48.8  $\mu\text{g}/\text{mL}$ ) than in the case of MB49 cells (concentrations of 9.8, 24.4, 48.8, and 97.5  $\mu\text{g}/\text{mL}$ ). Lipo3000 was found to be significantly less toxic in 22Rv1 cells when compared to the 24.4 and 48.8  $\mu\text{g}/\text{mL}$  concentration of the nanoassemblies. Lipo3000 demonstrated

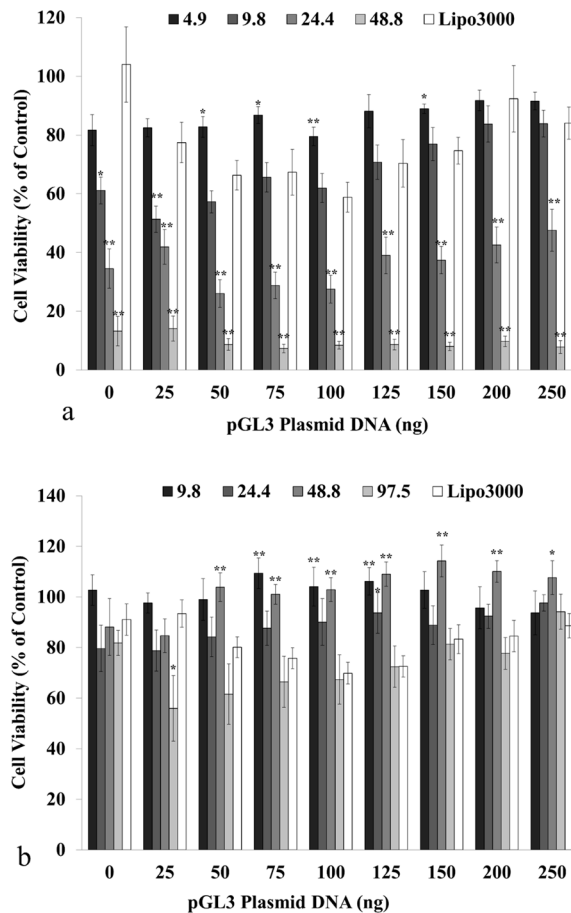


**Figure 9.** Viability of (a) 22Rv1 and (b) MB49 cells following treatment with 1,4C-1,4Bis-GNPs synthesized at a weight ratio of 100:1 of 1,4C-1,4Bis-PAE/HAuCl<sub>4</sub> in the presence of UV irradiation. The concentrations of 1,4C-1,4Bis-GNPs were adjusted to 4.9, 9.8, 24.4, and 48.8 µg/mL for 22Rv1 cells and 9.8, 24.4, 48.8, and 97.5 µg/mL in MB49 cells and loaded with different amounts of pGL3 plasmid DNA for transgene expression. Lipo3000 was also investigated as a control. Cell viability was determined 48 h after transfection (see the Experimental Section for details). Data points represent the mean measurement ± standard error ( $n \geq 3$ ). Statistical significance comparing GNP condition compared to Lipo3000 at the same plasmid loading amount is denoted by asterisks (Student's *t* test; \*,  $p \leq 0.05$ ; \*\*,  $p \leq 0.01$ ).

similar toxicity to that of nanoassemblies in a majority of cases in MB49 cells.

The highest observed luciferase transgene expression was ~9.2 million RLU/mg at 4.9 µg/mL of 1,4C-1,4Bis-GNPs and a plasmid loading of 25 ng in 22Rv1 cells (Figure 10a). These levels of luciferase expression were significantly higher to those observed with Lipo3000. Luciferase expression decreased with increasing plasmid loading on the nanoparticles when the 1,4C-1,4Bis-GNP concentration was maintained at 4.9 µg/mL. A similar trend was observed when 9.8 µg/mL GNPs were employed for delivering plasmid DNA. However, at this concentration, luciferase expression levels observed in 22Rv1 cells were significantly higher than those observed with Lipo3000 at plasmid DNA loading conditions of 50 and 75 ng. It is likely that the decrease in luciferase expression with increased loadings of plasmid DNA is due to a decrease in the nanoassembly zeta potential, because negatively charged plasmids can shield the positively charged polymer coating

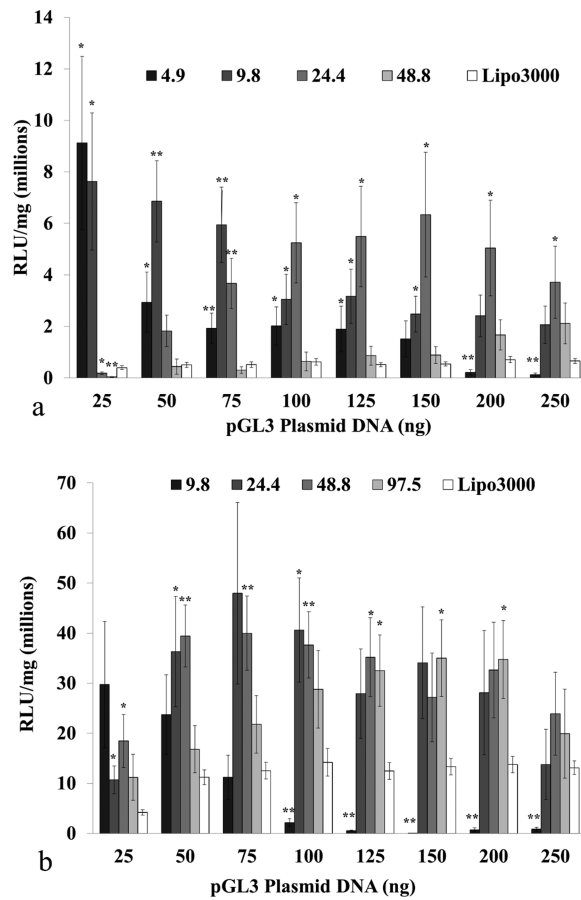


**Figure 10.** Luciferase transgene expression (RLU/mg) in (a) 22Rv1 and (b) MB49 cells following delivery of 1,4C-1,4Bis-GNPs synthesized at a weight ratio of 100:1 of 1,4C-1,4Bis to HAuCl<sub>4</sub> with UV irradiation. The concentrations of 1,4C-1,4Bis-GNPs were adjusted to 4.9, 9.8, 24.4, and 48.8 µg/mL for 22Rv1 cells and 9.8, 24.4, 48.8, and 97.5 µg/mL in MB49 cells, and loaded with different amounts of pGL3 plasmid DNA for transgene expression. Lipo3000 was also investigated as a control. Luciferase expression was determined 48 h after transfection (see the Experimental Section for details). Data points represent the mean measurement ± standard error ( $n \geq 3$ ). Statistical significance comparing GNP condition compared to Lipo3000 at the same plasmid loading amount is denoted by asterisks (Student's *t* test; \*,  $p \leq 0.05$ ; \*\*,  $p \leq 0.01$ ).

with increasing loading amounts, as seen previously,<sup>11</sup> reducing cell interactions and uptake. Zeta potential values of 1,4C-1,4Bis-GNPs were found to decrease for all nanoparticle concentrations as the loading of plasmid DNA increased to 250 ng (Figure 11). In some instances, a reversal of the positive charge was observed, likely due to excess negative charge of the plasmid DNA, which shields the positive charges from the amines in these PAEs.

Use of higher concentrations of 1,4C-1,4Bis-GNPs (i.e., 24.4, 48.8, and 97.5 µg/mL) can result in increased luciferase expression, most likely due to an increase in the effective polymer concentration. Although increased polymer concentration can allow for increased interactions with cells, leading to greater uptake, cell viability was observed to be less than 50% under these conditions. As a consequence of this toxicity at higher doses, luciferase expression levels did not reach the maximum observed in case of the 4.9 µg/mL nanoassembly condition.

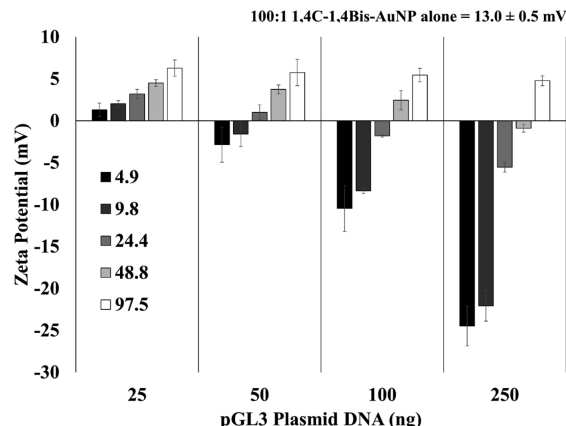


**Figure 11.** Zeta potential values of 1,4C–1,4Bis–GNPs synthesized at a weight ratio of 100:1 1,4C–1,4Bis to HAuCl<sub>4</sub> with UV irradiation, and subsequently loaded with varying amounts of pGGL3 plasmid DNA (ng plasmid DNA indicated in the figure legend). Values represent the mean zeta potential ± standard error ( $n = 3$ ). All plasmid loading conditions were found to have statistically significant difference compared to the unloaded condition (Student's *t* test,  $p < 0.05$ ).

In MB49 cells, the highest observed luciferase expression was ~50 million RLU/mg at a GNP concentration of 24.4  $\mu$ g/mL and plasmid loading of 75 ng (Figure 10b). However, this level of luciferase expression was not found to be statistically significant from that seen using Lipo3000. However, 1,4C–1,4Bis–GNPs exhibited a significantly higher transgene expression efficacy than Lipo3000 at concentrations of 48.8 and 97.5  $\mu$ g/mL. Additionally, the levels of luciferase expression observed in MB49 cells were significantly higher than those observed in 22Rv1 cells under comparable conditions. Luciferase expression levels decreased with increased plasmid DNA loading in MB49 cells, which was similar to the trend observed in 22Rv1 cells. As before, this is likely due to the observed decrease in zeta potential (Figure 11) caused by shielding of the positive charges on the PAEs by plasmid DNA.<sup>11</sup> It is likely that intermediate loadings of pGGL3 (25–100 ng) are likely ideal conditions where zeta potential is positive enough to allow for cell interaction and uptake, and enough plasmid DNA is loaded for effective transgene delivery and expression. A careful balance between plasmid DNA loading, subsequent transgene expression efficacy, and cytotoxicity therefore needs to be maintained for optimizing performance using polymer–nanoparticle nanoassemblies.

## ■ DISCUSSION

The facile synthesis method and chemical diversity of the poly(amino ether) polymers have elucidated certain design principles that could help in engineering future amine-containing polymeric systems for efficient one-pot synthesis of gold and silver nanoparticle systems. As can be observed from our results, polymers with higher amounts of tertiary amines resulted in the fastest nanoparticle growth. Similar observations have been reported, wherein increasing the ratio of tertiary amines to gold-salt resulted in a decrease in time for observable gold nanoparticle synthesis using PAMAM succinamic acid dendrimers.<sup>58</sup> The ability of tertiary amines to engender faster nanoparticle formation kinetics is likely due to two reasons. First, the binding of tertiary amines to metal ions is weaker than that of secondary or primary amines. This is important as it allows for binding, reduction, and quick release

of the metal ions for nucleation and nanoparticle growth. Second, tertiary amines have a higher oxidation potential than secondary or primary amines,<sup>59</sup> which allows for them to more readily give up electrons resulting in faster reduction of the metal ions. Although tertiary amines are favorable for reduction and release of metal ions, secondary and primary amines have the same function, only at slower rates. Thus, optimization of primary, secondary, and tertiary amines within a polymer can allow for tunability of nanoparticle growth, depending on specific requirements. It has been reported that change in nanoparticle reduction/nucleation rates can affect the size and optical properties of nanoparticles.<sup>60</sup> This change in nanoparticle formation rate can also be a result of reaction conditions. As observed here, an increase in polymer concentration led to the decrease in nanoparticle formation kinetics (Figure 3). This also shows the importance of using an appropriate capping agent that can not only stabilize nanoparticles in aqueous media, but also impart the desired functionality for a given application. Specifically, PAE-templated gold nanoparticles synthesized in this study were used for transgene delivery and expression. Thus, PAEs were simultaneously able to template nanoparticle formation, stabilize them in aqueous media, and carry and deliver plasmid DNA to mammalian (cancer) cells, leading to transgene expression.

PAE-templated gold and silver nanoparticle formation reported here is a facile and attractive method for synthesis of these plasmonic nanoassemblies, and is either competitive to or better than other existing methods employed for nanoparticle generation. Polypeptides have also been used as reducing and capping agents for facilitating nanoparticle formation from metal salts; it was found that the formation of metal nanoparticles by short peptides depends on both the reducing capability and the capping/binding properties of the peptide.<sup>42</sup> Polypeptide-nanoconjugates have been used to template the synthesis of gold nanoparticles in a one-pot method and have been used for transgene delivery<sup>43</sup> as well as antiviral and anticancer drug delivery<sup>61</sup> in vitro. We have previously demonstrated that cysteine-containing elastin-like polypeptides can be employed for templating the formation of gold nanoparticle synthesis within 18 h, although upward of 175 Gy of ionizing (X-ray) radiation are required for obtaining significant levels of nanoparticles.<sup>28</sup>

Polymers have also been investigated for the synthesis of gold nanoparticles. For example, PVP has been used as a capping agent for nanoparticles synthesized via reduction by glycerol.<sup>62</sup> Thiol-modified pEI2 (pEI with a molecular weight of 2 kDa) was used for capping gold nanoparticles following chemical reduction and demonstrated efficient gene delivery.<sup>12</sup> Chemical modifications were necessary to thiolate pEI, and NaBH<sub>4</sub> was required to induce nanoparticle formation. In addition, pEI25k–silver nanoparticles have been synthesized; however, they required additional chemical reduction or high temperatures for efficient nanoparticle synthesis.<sup>54,55</sup> PEI25k has been investigated previously for the one-pot synthesis of gold nanoparticles<sup>60</sup> and pEI25k–gold nanoparticles demonstrated efficient delivery of siRNA for gene silencing.<sup>31</sup> However, as demonstrated here and previously by us, several poly(amino ethers) demonstrate either higher transgene expression efficacies,<sup>11,35,37</sup> nanoparticle templating activities, or both, compared to pEI25k.

## CONCLUSIONS

In this study, we demonstrated a facile, one-pot, combinatorial synthesis method for the generation of both gold and silver nanoparticles under ambient conditions using a small set of poly(amino ethers) generated in our laboratory. PAEs were able to simultaneously act as both reducing and capping agents for nanoparticle synthesis and did not require the use of any additional reagents (e.g., reducing agents) or subsequent derivatization, all of which are significant advantages over several existing methods. Poly(amino ethers) from our library demonstrated faster kinetics of gold nanoparticle formation compared to 25 kDa branched poly(ethylene imine) or pEI25k. Significantly, all PAEs were able to template the formation of silver nanoparticles, whereas this was not observed with pEI25k.

The rate of nanoparticle formation is dependent on the chemical composition of the polyamine monomers used in the polymer synthesis. Particularly, 1,4-bis(3-aminopropyl) piperazine (1,4Bis), and 3,3'-diamino-N-methyldipropylamine (3,3')-based polymers, which are likely to have a high content of tertiary amines, demonstrated the fastest kinetics of nanoparticle formation, possibly due to increased solvation of amine-metal complexes that facilitates nanoparticle nucleation.<sup>42</sup> Nanoparticle synthesis was dependent on the polymer concentration relative to the metal ion concentration. Exposure to UV irradiation significantly enhanced the kinetics of nanoparticle formation; of particular significance, the time required for silver nanoparticle synthesis was greatly reduced from several days to only a few minutes in the presence of UV radiation. Hydrodynamic diameters of less than 150 nm were seen for all nanoparticles, while the metal cores were spherical and approximately 20 nm in diameter in most cases. We demonstrated that 1,4C–1,4Bis-templated gold nanoparticles were able to deliver plasmid DNA leading to transgene (luciferase) expression in two different cancer cell lines. The ease of synthesis of PAE-templated plasmonic nanoparticles, stability in biologically relevant media, presence of amines for further functionalization, and biological activity (e.g., nucleic acid delivery) make this an attractive approach for several applications in biotechnology and medicine.

## ASSOCIATED CONTENT

### Supporting Information

Kinetics of GNP and AgNP formation templated by NPGDE-derived PAEs and formation of PSS-templated GNP. This material is available free of charge via the Internet at <http://pubs.acs.org>.

## AUTHOR INFORMATION

### Corresponding Author

\*E-mail: kaushal.rege@asu.edu. Fax: 480-727-3292. Phone: 480-727-8616.

### Notes

The authors declare no competing financial interest.

## ACKNOWLEDGMENTS

The authors are grateful to the National Science Foundation (Grant CBET-0829128) and the National Institute of General Medical Sciences, NIH (Grant 1R01GM093229-01A1), for funding this research. J.R. is also grateful to the Achievement Rewards for College Scientists (ARCS) fellowship. O.S. acknowledges support from the National Nanotechnology

Infrastructure Network (NNIN) REU Program funded by the National Science Foundation under Grant No. ECCS-0335765.

## REFERENCES

- (1) Ghosh, P.; Han, G.; De, M.; Kyu Kim, C.; Rotello, V. M. Gold Nanoparticles in Delivery Applications. *Adv. Drug Delivery Rev.* **2008**, *60*, 1307–1315.
- (2) Huang, H. C.; Barua, S.; Sharma, G.; Dey, S. K.; Rege, K. Inorganic Nanoparticles for Cancer Imaging and Therapy. *J. Controlled Release* **2011**, *155*, 344–57.
- (3) Wang, T.; Mancuso, J.; Kazmi, S.; Dwelle, J.; Sapozhnikova, V.; Willsey, B.; Ma, L.; Qiu, J.; Li, X.; Dunn, A.; Johnston, K.; Feldman, M.; Milner, T. Combined Two-Photon Luminescence Microscopy and OCT for Macrophage Detection in the Hypercholesterolemic Rabbit Aorta Using Plasmonic Gold Nanorose. *Lasers Surg. Med.* **2012**, *1*, 49–45.
- (4) Gross, G.; Nelson, D.; Grate, J.; Synovec, R. Monolayer-Protected Gold Nanoparticles as a Stationary Phase for Open Tubular Gas Chromatography. *Anal. Chem.* **2003**, *75*, 4558–4564.
- (5) Dos Santos, D. S., Jr.; Goulet, P.; Pieczonka, N.; Oliveira, O. J.; Aroca, R. Gold Nanoparticle Embedded, Self-Sustained Chitosan Films as Substrates for Surface-Enhanced Raman Scattering. *Langmuir* **2004**, *20*, 10273–10277.
- (6) Faulds, K.; Littleford, R.; Graham, D.; Dent, G.; Smith, W. Comparison of Surface-Enhanced Resonance Raman Scattering from Unaggregated and Aggregated Nanoparticles. *Anal. Chem.* **2004**, *76*, 592–598.
- (7) Ramos, J.; Taylor, D.; Rege, K. Gold Nanoparticle Mediated Photo-Chemotherapy. *J. Nanomed. Nanotechnol.* **2012**, *3*, 1000e125.
- (8) Kim, S. T.; Chompoosor, A.; Yeh, Y.-C.; Agasti, S. S.; Solfield, D. J.; Rotello, V. M. Dendronized Gold Nanoparticles for siRNA Delivery. *Small* **2012**, *8*, 3253–3256.
- (9) Conde, J.; Ambrosone, A.; Sanz, V.; Hernandez, Y.; Marchesano, V.; Tian, F.; Child, H.; Berry, C. C.; Ibarra, M. R.; Baptista, P. V.; Tortiglione, C.; de la Fuente, J. M. Design of Multifunctional Gold Nanoparticles for in Vitro and in Vivo Gene Silencing. *ACS Nano* **2012**, *6*, 8316–8324.
- (10) Hu, C.; Peng, Q.; Chen, F.; Zhong, Z.; Zhuo, R. Low Molecular Weight Polyethylenimine Conjugated Gold Nanoparticles as Efficient Gene Vectors. *Bioconjugate Chem.* **2010**, *20*, 836–844.
- (11) Ramos, J.; Rege, K. Transgene Delivery using Poly(amino ether)-Gold Nanorod Assemblies. *Biotechnol. Bioeng.* **2012**, *109*, 1336–1436.
- (12) Thomas, M.; Klibanov, A. M. Conjugation to Gold Nanoparticles Enhances Polyethylenimine's Transfer of Plasmid DNA into Mammalian Cells. *Proc. Natl. Acad. Sci. U.S.A.* **2003**, *100*, 9138–9143.
- (13) Huang, H.-C.; Ramos, J.; Grandhi, T. S. P.; Potta, T.; Rege, K. Gold Nanoparticles in Cancer Imaging and Therapeutics. *Nano LIFE* **2010**, *01*, 289–307.
- (14) Sokolov, K.; Follen, M.; Aaron, J.; Pavlova, I.; Malpica, A.; Lotan, R.; Richards-Kortum, R. Real-Time Vital Optical Imaging of Precancer Using Anti-Epidermal Growth Factor Receptor Antibodies Conjugated to Gold Nanoparticles. *Cancer Res.* **2003**, *63*, 1999–2004.
- (15) Bardhan, R.; Lal, S.; Joshi, A.; Halas, N. J. Theranostic Nanoshells: From Probe Design to Imaging and Treatment of Cancer. *Acc. Chem. Res.* **2011**, *44*, 936–946.
- (16) Huang, X.; Neretina, S.; El-Sayed, M. Gold Nanorods: From Synthesis and Properties to Biological and Biomedical Applications. *Adv. Biomater.* **2009**, *27*, 1–31.
- (17) You, C.; Han, C.; Wang, Z.; Zheng, Y.; Li, Q.; Hu, X.; Sun, H. The Progress of Silver Nanoparticles in the Antibacterial Mechanism, Clinical Application, and Cytotoxicity. *Mol. Biol. Rep.* **2012**, *39*, 9193–9201.
- (18) Esteban-Tejada, L.; Malpartida, F.; Esteban-Cubillo, A.; Pecharroman, C.; Moya, J. S. The Antibacterial and Antifungal Activity of a Soda-Lime Glass Containing Silver Nanoparticles. *Nanotechnology* **2009**, *20*.
- (19) Panacek, A.; Kolar, M.; Vacerova, R.; Prucek, R.; Soukupova, J.; Krystof, V.; Hamal, P.; Zboril, R.; Kvitek, L. Antifungal Activity of

- Silver Nanoparticles Against *Candida*. *Biomaterials* **2009**, *30*, 6333–6340.
- (20) Singh, S.; D'Britto, V.; Prabhune, A. A.; Ramana, C. V.; Dhawan, A.; Prasad, B. L. V. Cytotoxic and Genotoxic Assessment of Glycolipid-Reduced and -Capped Gold and Silver Nanoparticles. *New J. Chem.* **2010**, *34*, 294–301.
- (21) Sotiriou, G. A.; Pratsinis, S. E. Engineering Nanosilver as an Antibacterial, Biosensor, and Bioimaging Material. *Curr. Opin. Chem. Eng.* **2011**, *1*, 3–10.
- (22) Nguyen, D. T.; Kim, D.-J.; So, M. G.; Kim, K.-S. Experimental Measurements of Gold Nanoparticle Nucleation and Growth by Citrate Reduction of HAuCl<sub>4</sub>. *Adv. Powder Technol.* **2010**, *21*, 111–118.
- (23) Shimmin, R. G.; Schoch, A. B.; Braun, P. V. Polymer Size and Concentration Effects on the Size of Gold Nanoparticles Capped by Polymeric Thiols. *Langmuir* **2004**, *20*, 5613–5620.
- (24) Al-Thabaiti, S. A.; Al-Nowaiser, F. M.; Obaid, A. Y.; Al-Youbi, A. O.; Khan, Z. Formation and Characterization of Surfactant Stabilized Silver Nanoparticles: A Kinetic Study. *Colloids Surf., B* **2008**, *67*, 230–237.
- (25) Eustis, S.; Hsu, H.-Y. H.; El-Sayed, M. A. Gold-Nanoparticle Formation from Photochemical Reduction of Au<sup>3+</sup> by Continuous Excitation in Colloidal Solutions. A Proposed Molecular Mechanism. *J. Phys. Chem. B* **2005**, *109*, 4811–4815.
- (26) Eustis, S.; El-Sayed, M. A. Molecular Mechanism of the Photochemical Generation of Gold Nanoparticles in Ethylene Glycol: Support for the Disproportionation Mechanism. *J. Phys. Chem. B* **2006**, *110*, 14014–14019.
- (27) Jia, H.; Zeng, J.; Song, W.; An, J.; Zhao, B. Preparation of Silver Nanoparticles by Photo-reduction for Surface-Enhanced Raman Scattering. *Thin Solid Films* **2006**, *496*, 281–287.
- (28) Walker, C. R.; Pushpavananam, K.; Nair, D. G.; Potta, T.; Sutiyoso, C.; Kodibagkar, V. D.; Sapareto, S.; Chang, J.; Rege, K. Generation of Polypeptide-Templated Gold Nanoparticles using Ionizing Radiation. *Langmuir* **2013**, *29*, 10166–10173.
- (29) Newman, J. D. S.; Blanchard, G. J. Formation of Gold Nanoparticles Using Amine Reducing Agents. *Langmuir* **2006**, *22*, 5882–5887.
- (30) Sakai, T.; Alexandridis, P. Mechanism of Gold Metal Ion Reduction, Nanoparticle Growth, and Size Control in Aqueous Amphiphilic Block Copolymer Solutions at Ambient Conditions. *J. Phys. Chem. B* **2005**, *109*, 7766–7777.
- (31) Song, W. J.; Du, J. Z.; Sun, T. M.; Zhang, P. Z.; Wang, J. Gold Nanoparticles Capped with Polyethyleneimine for Enhanced siRNA Delivery. *Small* **2010**, *6*, 239–246.
- (32) Bhargava, S.; Booth, J.; Agrawal, S.; Coloe, P.; Kar, G. Gold Nanoparticle Formation During Bromoaurate Reduction by Amino Acids. *Langmuir* **2005**, *21*, 5949–5956.
- (33) Selvakannan, P.; Mandal, S.; Phadtare, S.; Gole, A.; Pasricha, R.; Adyanthaya, S.; Sastry, M. Water-Dispersible Tryptophan-Protected Gold Nanoaprticles Prepared by the Spontaneous Reduction of Aqueous Chloroaurate Ions by the Amino Acid. *J. Colloid Interface Sci.* **2004**, *269*, 97–102.
- (34) Newman, J. D. S.; Blanchard, G. J. Formation and Encapsulation of Gold Nanoaprticles Using a Polymeric Amine Reducing Agent. *J. Nanopart. Res.* **2007**, *9*, 861–868.
- (35) Barua, S.; Joshi, A.; Banerjee, A.; Matthews, D.; Sharfstein, S. T.; Cramer, S. M.; Kane, R. S.; Rege, K. Parallel Synthesis and Screening of Polymers for Nonviral Gene Delivery. *Mol. Pharmaceutics* **2009**, *6*, 86–97.
- (36) Barua, S.; Ramos, J.; Potta, T.; Taylor, D.; Huang, H. C.; Montanez, G.; Rege, K. Discovery of Cationic Polymers for Non-Viral Gene Delivery Using Combinatorial Approaches. *Comb. Chem. High Throughput Screening* **2011**, *10*, 908–924.
- (37) Vu, L.; Ramos, J.; Potta, T.; Rege, K. Generation of a Focused Poly(Amino Ether) Library: Polymer-Mediated Transgene Delivery and Gold-Nanorod Based Theranostic Systems. *Theranostics* **2012**, *2*, 1160–1173.
- (38) Kasman, L. M.; Barua, S.; Lu, P.; Rege, K.; Voelkel-Johnson, C. Polymer-Enhanced Adenoviral Transduction of CAR-Negative Bladder Cancer Cells. *Mol. Pharmaceutics* **2009**, *6*, 1612–1619.
- (39) Gosnell, H.; Kasman, L.; Potta, T.; Vu, L.; Garrett-Mayer, E.; Rege, K.; Voelkel-Johnson, C. Polymer-Enhanced Delivery Increases Adenoviral Gene Expression in an Orthotopic Model of Bladder Cancer. *J. Controlled Release* **2014**, *176*, 35–43.
- (40) Hayon, T.; Dvilkansky, A.; Shpilberg, O.; Nathan, I. Appraisal of the MTT-Based Assay as a Useful Tool for Predicting Drug Chemosensitivity in Leukemia. *Leuk. Lymphoma* **2003**, *44*, 1957–1962.
- (41) Golub, G.; Zilberman, I.; Cohen, H.; Meyerstein, D. Tertiary-poly-amine Ligands as Stabilizers of Transition Metal Complexes with Uncommon Oxidation States. *Supramol. Chem.* **1996**, *6*, 275–279.
- (42) Tan, Y. N.; Lee, J. Y.; Wang, D. I. C. Uncovering the Design Rules for Peptide Synthesis of Metal Nanoparticles. *J. Am. Chem. Soc.* **2010**, *132*, 5677–5686.
- (43) Yan, X.; Blacklock, J.; Li, J.; Mohwald, H. One-Pot Synthesis of Polypeptide-Gold Nanoconjugates for in Vitro Gene Transfection. *ACS Nano* **2012**, *6*, 111–117.
- (44) Li, C.; Li, D.; Wan, G.; Xu, J.; Hou, W. Facile Synthesis of Concentrated Gold Nanoparticles with Low Size-Distribution in Water: Temperature and pH Controls. *Nanoscale Res. Lett.* **2011**, *6*, 440.
- (45) Mualidharan, G.; Subramanian, L.; Nallamuthu, S. K.; Santhanam, V.; Kumar, S. Effect of Reagent Addition Rate and Temperature on Synthesis of Gold Nanoparticles in Microemulsion Route. *Ind. Eng. Chem. Res.* **2011**, *50*, 8786–8791.
- (46) Harada, M.; Inada, Y.; Nomura, M. In Situ Time-Resolved XAFS Analysis of Silver Particle Formation by Photoreduction in Polymer Solutions. *J. Colloid Interface Sci.* **2009**, *337*, 427–438.
- (47) Zhang, H.; Huang, X.; Li, L.; Hussain, I.; Li, Z.; Tan, B. Photoreductive Synthesis of Water-Soluble Fluorescent Metal Nano-clusters. *Chem. Commun. (Cambridge, U.K.)* **2012**, *48*, 567–569.
- (48) Kurihara, K.; Kizling, J.; Stenius, P.; Fendler, J. Laser and Pulse Radiolytically Induced Colloidal Gold Formation in Water and in Water-in-Oil Microemulsions. *J. Am. Chem. Soc.* **1983**, *105*, 2574–2579.
- (49) Kumar, S.; Kumar, C.; Mathiyarasu, J.; Phani, K. Stabilized Gold Nanoparticles by Reduction Using 3,4-Ethylenedioxythiophene-polystyrenesulfonate in Aqueous Solutions: Nanocomposite Formation, Stability, and Application in Catalysis. *Langmuir* **2007**, *23*, 3401–3408.
- (50) Dorris, A.; Rucareanu, S.; Reven, L.; Barrett, C.; Lennox, R. Preparation and Characterization of Polyelectrolyte-Coated Gold Nanoparticles. *Langmuir* **2008**, *18*, 2532–2538.
- (51) Hu, C.; Huang, Y.; Tsang, R. Thermal and Spectroscopic Properties of Polystyrene/Gold Nanocomposite Containing Well Dispersed Nanoparticles. *J. Nanosci. Nanotechnol.* **2009**, *9*, 3084–3091.
- (52) Nath, S.; Ghosh, S. K.; Kundu, S.; Praharaj, S.; Panigrahi, S.; Pal, T. Is Gold Really Softer than Silver? HSAB Principle Revisited. *J. Nanopart. Res.* **2006**, *8*, 111–116.
- (53) Hoppe, C. E.; Lazzari, M.; Pardinas-Blanco, I.; Lopez-Quintela, M. A. One-Step Synthesis of Gold and Silver Hydrosols Using Poly(V-vinyl-2-pyrrolidone) as a Reducing Agent. *Langmuir* **2006**, *22*, 7027–7034.
- (54) Lee, H.; Lee, S.; Oh, E.; Chung, H.; Han, S.; Kim, E.; Seo, S.; Ghim, H.; Yeum, J.; Choi, J. Antimicrobial Polyethyleneimine-Silver Nanoparticle in a Stable Colloidal Dispersion. *Colloids Surf., B* **2001**, *88*, 505–511.
- (55) Shin, K. S.; Kim, J. H. One-Step Fabrication of Poly(ethylenimine)-Stabilized Silver Nanoparticles from Insoluble Silver Chloride Salt. *Bull. Korean Chem. Soc.* **2011**, *32*, 2469–2472.
- (56) Barua, S.; Rege, K. The Influence of Mediators of Intracellular Trafficking on Transgene Expression Efficacy of Polymer-Plasmid DNA Complexes. *Biomaterials* **2010**, *31*, 5894–8902.
- (57) Ramos, J.; Rege, K. Poly(aminoether)-Gold Nanorod Assemblies for shRNA Plasmid-Induced Gene Silencing. *Mol. Pharmaceutics* **2013**, *10*, 4107–4119.

- (58) Vasile, E.; Serafim, A.; Petre, D.; Giol, D.; Dubruel, P.; Iovu, H.; Stancu, I. C. Direct Synthesis and Morphological Characterization of Gold-Dendrimer Nanocomposites Prepared Using PAMAM Succinamic Acid Dendrimers: Preliminary Study of the Calcification Potential. *Sci. World J.* **2014**, 103462.
- (59) Lewis, F.; Crompton, E. SET Addition of Amines to Alkenes. In *CRC Handbook of Organic Photochemistry and Photobiology*; Horspool, W., Lenci, F., Eds.; CRC Press: Boca Raton, FL, 2004; Chapter 7.
- (60) Sun, X.; Dong, S.; Wang, E. One-Step Preparation of Highly Concentrated Well-Stable Gold Colloids by Direct Mix of Polyelectrolyte and HAuCl<sub>4</sub> Aqueous Solutions at Room Temperature. *J. Colloid Interface Sci.* **2005**, 288, 301–303.
- (61) Shirazi, A. N.; Mandal, D.; Tiwari, R. k.; Guo, L.; Lu, W.; Parang, K. Cyclic Peptide-Capped Gold Nanoaprticles as Drug Delivery Systems. *Mol. Pharmacol.* **2012**, 10, 500–511.
- (62) Grace, A. N.; Pandian, K. One-Pot Synthesis of Polymer Protected Gold Nanoaprticles and Nanoprisms in Glycerol. *Colloids Surf, A* **2006**, 290, 138–142.